

pubs.acs.org/chemneuro Research Article

# $\alpha$ S Oligomers Generated from Interactions with a Polyunsaturated Fatty Acid and a Dopamine Metabolite Differentially Interact with A $\beta$ to Enhance Neurotoxicity

Shailendra Dhakal, Jhinuk Saha, Courtney E. Wyant, and Vijayaraghavan Rangachari\*



Cite This: ACS Chem. Neurosci. 2021, 12, 4153-4161



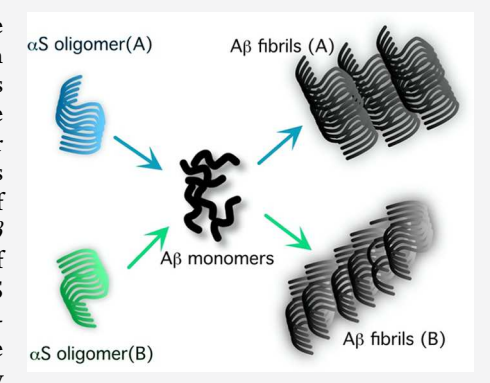
**Read Online** 

# **ACCESS**

III Metrics & More

Article Recommendations

**ABSTRACT:** It is increasingly becoming clear that neurodegenerative diseases are not as discrete as originally thought to be but display significant overlap in histopathological and clinical presentations. For example, nearly half of the patients with Alzheimer's disease (AD) and synucleinopathies such as Parkinson's disease (PD) show symptoms and pathological features of one another. Yet, the molecular events and features that underlie such comorbidities in neurodegenerative diseases remain poorly understood. Here, inspired to uncover the molecular underpinnings of the overlap between AD and PD, we investigated the interactions between amyloid- $\beta$  (A $\beta$ ) and  $\alpha$ -synuclein ( $\alpha$ S), aggregates of which form the major components of amyloid plaques and Lewy bodies, respectively. Specifically, we focused on  $\alpha$ S oligomers generated from the dopamine metabolite called dihydroxyphenylacetaldehyde (DOPAL) and a polyunsaturated fatty acid docosahexaenoic acid (DHA). The two  $\alpha$ S oligomers showed structural and conformational differences as confirmed by



the disparity in size, secondary structure, susceptibility to proteinase K digestion, and cytotoxicity. More importantly, the two oligomers differentially modulated  $A\beta$  aggregation; while both inhibited  $A\beta$  aggregation to varying extents, they also induced structurally different  $A\beta$  assemblies. Furthermore,  $A\beta$  seeded with DHA-derived  $\alpha$ S oligomers showed greater toxicity than DOPAL-derived  $\alpha$ S oligomers in SH-SY5Y neuroblastoma cells. These results provide insights into the interactions between two amyloid proteins with empirically distinctive biophysical and cellular manifestations, enunciating a basis for potentially ubiquitous cross-amyloid interactions across many neurodegenerative diseases.

KEYWORDS: DOPAL, DHA,  $\alpha S$  oligomers,  $A\beta$ , Alzheimer's disease, Parkinson's disease.

# INTRODUCTION

Aggregates of amyloid- $\beta$  (A $\beta$ ) and  $\alpha$ -synuclein ( $\alpha$ S) constitute the major components of extracellular plaques and intracellular Lewy bodies that are the hallmarks of Alzheimer's disease (AD) and Parkinson's disease (PD), respectively. However, it is increasingly becoming clear that amyloid depositions in neurodegenerative diseases are seldom discrete and show significant overlap clinically and histopathologically. 1-3 This is particularly the case with sporadic or familial AD and PD, where up to 50% of patients from one pathology show the symptoms of the other.<sup>4</sup> In familial AD, deposits of A $\beta$  are often observed alongside Lewy bodies comprised of  $\alpha$ S.<sup>5,6</sup> Despite the pathological overlaps and comorbidities, the molecular reasons behind copathological presentations in neurodegenerative diseases remain unclear. A $\beta$  peptides (40 and 42) are primarily generated in the extracellular space upon sequential cleavage of amyloid precursor protein (APP) by the aspartyl proteases,  $\beta$ - and  $\gamma$ -secretases. Though A $\beta$ 42 is more aggressive than A $\beta$ 40 in terms of aggregation and toxicity, both forms of the protein are present in the plaque deposits. Implicated primarily in AD, A $\beta$  aggregates are also observed in many other neurodegenerative pathologies including PD, amyotrophic lateral sclerosis (ALS), frontotemporal lobar degeneration (FTLD), and prion disease. 10-14 Similarly,  $\alpha$ S's involvement is also not limited to PD but observed in a wide spectrum of synucleinopathies such as multiple system atrophy (MSA), dementia with Lewy bodies (DLB) as well as in AD and ALS. 15-18 Previous clinical studies have shown the cooccurrence of  $\alpha$ S and A $\beta$  aggregates within the neocortical regions during the late stages of neurodegenerative pathologies. Brain autopsies have also revealed overlapping DLB/PD cases in clinically confirmed AD cases with characteristic A $\beta$ / tau aggregates. Peciphering the molecular underpinnings in copathologies will require deeper investigations into the cross-

Received: August 13, 2021 Accepted: October 8, 2021 Published: October 19, 2021





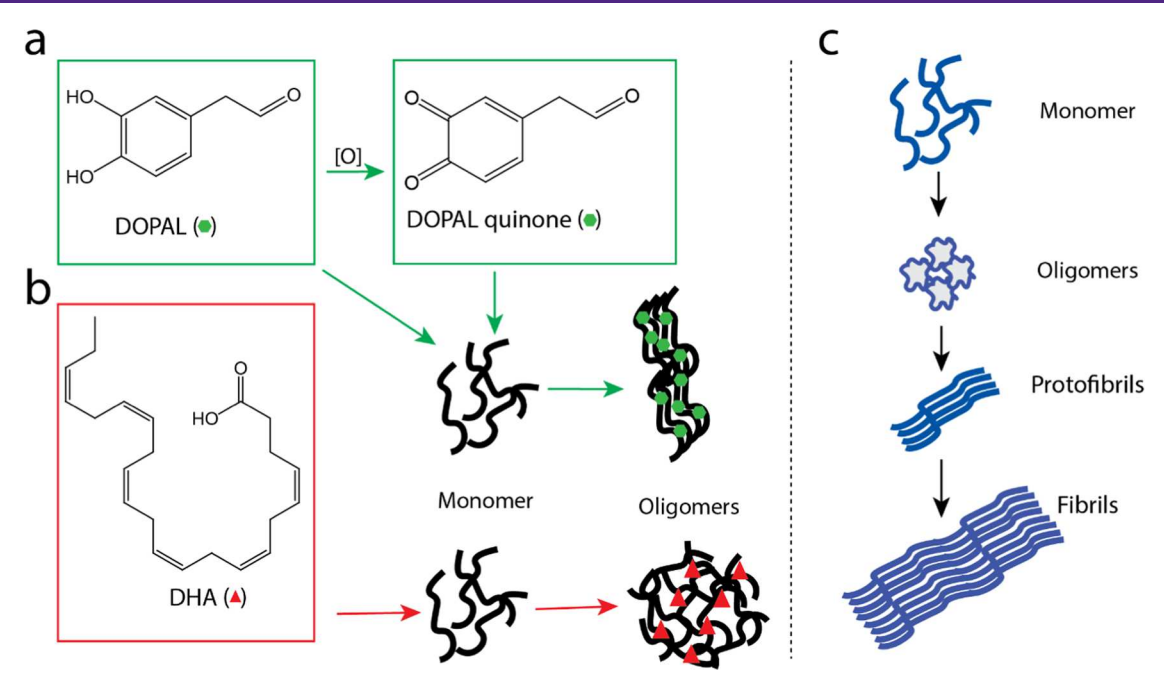


**Figure 1.** Schematic diagram showing on-pathway and off-pathway  $\alpha$ S aggregation. (a) DOPAL forms DOPAL quinone in the oxidizing environment, which interacts with  $\alpha$ S monomers both covalently and noncovalently resulting in oligomer formation. In the reduced form, it can form Schiff's base with  $\alpha$ S monomers to form oligomers. (b) DHA can interact with  $\alpha$ S monomers through oxidative modification at four methionine residues and covalent carbonyl adduct formation at protein side chains to form structurally distinct  $\alpha$ S oligomers. (c) Schematics of on-pathway  $\alpha$ S aggregation resulting in oligomer, protofibril, and fibril formation.

talks between multiple amyloidogenic proteins and to elucidate selectivity in such interactions. These have propelled in vitro studies, some of which show direct interactions between monomeric  $\alpha S$  and  $A\beta$  resulting in the cross-seeding and fibril formation.<sup>20</sup> We also showed the cross interaction of dopamine-derived  $\alpha$ S oligomers (DSOs) with A $\beta$ 42 monomers resulting in higher-molecular-weight oligomer formation.<sup>21</sup> A more recent study has shown that  $\alpha S$  oligomers generated from dopamine and those derived from the polyunsaturated fatty acid, docosahexaenoic acid (DHA), show mesoscale differences.<sup>22</sup> In addition, the two oligomers exhibited differential cross-interactions with tau leading to diverse biophysical characteristics and cytotoxic events.<sup>22</sup> Since the variations in oligomer conformations and fibril polymorphisms among amyloid species are emerging to be a key contributor for the observed phenotypes and clinical presentations, 23-25 the investigations into a deeper understanding of oligomers becomes imperative.

Based on the cues from the effect on tau, we investigated the effects of 3,4-dihydroxyphenylacetaldehyde (DOPAL) and DHA-derived  $\alpha S$  oligomers (from here on, DOPAL-SOs and DHA-SOs, respectively) on  $A\beta$  aggregation. We hypothesized that these oligomers of  $\alpha S$  may cross-interact with  $A\beta$  monomers causing alteration of the latter aggregation and toxicity. DOPAL is a monoamine oxidase (MAO)-derived metabolite of dopamine, which is toxic to the neurons at physiological concentrations.  $^{22,26-28}$  It is shown to be associated with damage of synaptic vesicles. Moreover, injection of DOPAL in rats led to the loss of dopaminergic neurons with an accumulation of  $\alpha S$  oligomers. The generation of  $\alpha S$  oligomers in the presence of DOPAL involves Schiff's base and Michael addition mechanisms with the free amines in  $\alpha S$  (N-terminus and lysines) to form covalent adducts (Figure 1a). On the other hand, DHA, a

major component of myelin sheath, is a polyunsaturated fatty acid with diverse physiological functions. Upon incubation with  $\alpha S$  monomers, DHA is shown to form both covalent adducts and engage in noncovalent interactions to generate oligomers with  $\alpha$ -helical characteristics<sup>30</sup> (Figure 1b). However, the oligomer displays a random coil structure with a decrease in DHA content within the oligomers. 30,31 In this study, we show that DOPAL-SOs and DHA-SOs are conformationally distinct with different biophysical characteristics. Our results indicate that the two  $\alpha S$  oligomers differentially interact with  $A\beta$  to inhibit its aggregation and generate species with distinct conformations, biophysical properties. More importantly, the two oligomers promote  $A\beta$ aggregate species that enhances cytotoxicity than the unseeded A $\beta$  control, demonstrating the ability of the  $\alpha$ S oligomers to induce  $A\beta$  aggregates with distinctive cellular responses.

# ■ RESULTS AND DISCUSSION

DOPAL and DHA-Derived  $\alpha$ S Oligomers Show Biophysical Differences. As mentioned above, DOPAL and DHA are known to form covalent adducts with  $\alpha S$ generating oligomers, which we suspected to be conformationally discrete to one another with distinctive properties. The chemistry of DOPAL is fairly well understood; in the reduced form, DOPAL forms a Schiff's base with the lysines in  $\alpha$ S and converts to a quinone form upon oxidation. This DOPAL- $\alpha$ S adduct then covalently or noncovalently interact with other  $\alpha S$ monomers to form oligomers.<sup>28</sup> DHA, on the other hand, is known to covalently interact with  $\alpha S$  monomers and promote oligomerization.<sup>22,31</sup> These are characterized as "off-pathway" oligomers of  $\alpha S$  that are not only temporally different from "on-pathway" counterparts but also structurally 31,32 (Figure 1). To investigate the properties of DOPAL-SOs and DHA-SOs, seed-free aS monomers were incubated with DOPAL and

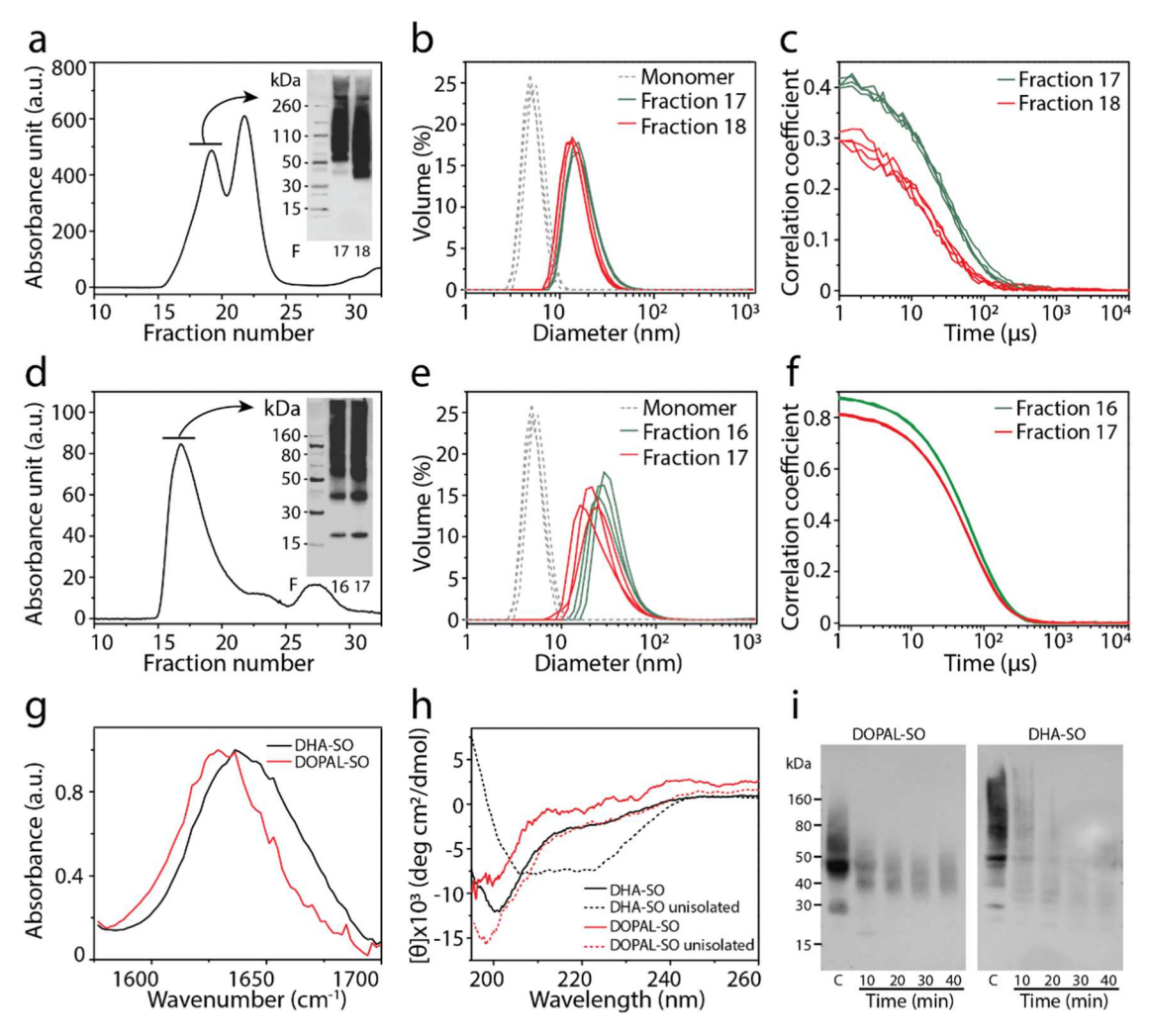


Figure 2. Isolation and characterization of DOPAL-SOs and DHA-SOs. (a) Size exclusion chromatogram of DOPAL-SOs along with immunoblots (inset) of fractions 17 and 18 (indicated by arrow) using  $\alpha$ S Syn211 antibody. (b, c) Hydrodynamic diameter of monomers and respective oligomers using DLS (b) and correlation coefficient (derived from autocorrelation function) of the respective oligomers plotted as a function of time (c). (d) Size exclusion chromatogram of DHA-SOs with immunoblots (inset) of fractions 16 and 17. (e, f) Hydrodynamic diameter of monomers and oligomeric fractions represented as volume percentage (e) and their correlation coefficient as a function of time (f). (g, h) Normalized FTIR and far-UV CD spectra of isolated DOPAL-SOs and DHA-SOs. (h) Black dotted lines and red dotted lines represent DHA-SOs and DOPAL-SOs, respectively, prior to SEC isolation. (i) Immunoblot showing PK digestion data of DOPAL-SOs and DHA-SOs at 10, 20, 30, and 40 min of incubation; C represents control oligomers without PK treatment.

DHA in separate reactions with orbitally shaking at physiological temperature. After 24 h, DOPAL-SOs were fractionated from the coincubated sample of DOPAL and  $\alpha$ S using size exclusion chromatography (SEC), which showed two distinguishable peaks between fractions 16-20 and 21-23 (Figure 2a). The first peak corresponding to fractions 17 and 18 showed the presence of a mixture of oligomers ranging between 50-260 and 36-260 kDa disperse bands, respectively (inset, Figure 2a). The second peak corresponding to fractions 21-23 revealed the presence of monomeric and dimeric species in SDS-PAGE gel (data not shown). Size analysis of the fractions 17 and 18 by dynamic light scattering (DLS) showed monodispersed peaks with a mean hydrodynamic diameter ranging from 10 to 40 nm, while the corresponding monomers showed 3-6 nm hydrodynamic diameter indicating the presence of some low-molecular-weight oligomeric species possibly dimers or trimers (Figure 2b). This is also captured in the autocorrelation function with the correlation coefficient for fraction 17 showing a slightly longer correlation time as

compared to fraction 18 reflecting a slightly larger size of the former than the latter (Figure 2c). SEC fractionation of DHA-SOs also showed a large peak near the excluded volume ranging from fractions 15 to 20 along with a small peak near the fraction numbers 25–30 corresponding to the monomers (Figure 2d). Immunoblotting of fractions 16 and 17 revealed a wide distribution of oligomeric species populated throughout the higher-molecular-weight region as compared to DOPAL-SOs (inset, Figure 2d). Corresponding DLS also showed wide size distribution with the mean hydrodynamic diameter ranging from 20 to 80 nm (Figure 2e). Among the two, fraction 16 showed a slightly large size as expected as compared to fraction 17 (Figure 2e,f).

Secondary structure of these oligomers was studied using Fourier transform infrared spectroscopy (FTIR) and far-UV circular dichroism (CD) spectroscopy. FTIR spectra revealed the random coiled, largely disordered structure of DOPAL-derived  $\alpha$ S oligomers with peak at  $\sim$ 1640 nm, while DHA-generated  $\alpha$ S oligomers showed peaks at 1640 and 1650 nm,

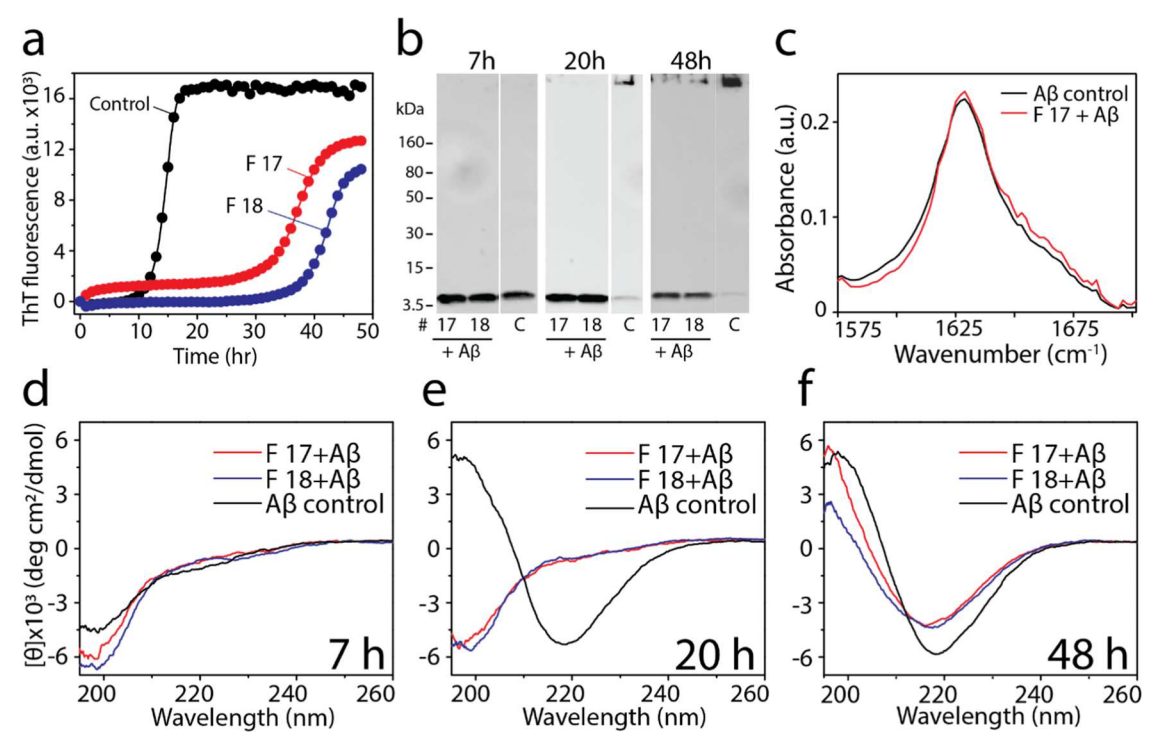


Figure 3. Interaction of DOPAL-SOs with  $A\beta$ . (a) ThT fluorescence kinetics of 15 μM  $A\beta$  monomers (black) alone and in the presence of 0.75 μM DOPAL-SO corresponding to 17 (red) and 18 (blue) fraction numbers in 20 mM Tris buffer pH 8.0. (b) Immunoblot of ThT reactions (a) at 7, 20, and after 48 h; C indicates the  $A\beta$  control sample. (c) FTIR analysis of reactions containing  $A\beta$  monomer (15 μM) alone and in the presence of 0.75 μM DOPAL-SOs (fraction 17) after 48 h. (d–f) CD spectra of ThT reactions (a) at 7, 20, and after 48 h, respectively.

indicating the presence of a randomly coiled structure with some  $\alpha$ -helical characteristics (Figure 2g). CD spectra of the oligomers showed subtly different secondary structures. Both SEC-isolated (red) and non-isolated (red dash lines) DOPAL-SOs exhibited spectra corresponding minima at 195 nm characteristics of a randomly coiled structure (Figure 2h), which is similar to the dopamine-derived oligomers. 21 DHAderived oligomers showed different secondary structures based on the degree of DHA associated with the protein. While SECisolated oligomers without free DHA showed mainly a random coiled structure with a minimum at 195 nm (black; Figure 2h), when complexed with DHA prior to SEC isolation, the sample displayed  $\alpha$ -helical characteristics with a minimum at 208 and a shoulder at 222 nm (black dash lines; Figure 2h), which is the form widely reported in the literature. 22,30,31,33-35 Finally, enzymatic stability of  $\alpha S$  oligomers was probed by proteinase K (PK) digestion. Stability of the oligomers was assessed by the disappearance of oligomeric band in immunoblots upon treatment with PK, digested at specific time intervals of 10, 20, 30, and 40 min. The samples were then run on SDS-PAGE gel and visualized by immunoblot using monoclonal anti- $\alpha S$ (Syn211) antibody. Upon doing so, the intensities of the bands for both DOPAL and DHA-derived  $\alpha S$  oligomers were diminished significantly compared to the controls within 10 min of PK digestion (Figure 2i). However, the intensity of DHA-derived  $\alpha$ S oligomers is found to be much lower than the intensity of DOPAL-derived  $\alpha$ S oligomers (Figure 2i). This indicates a higher susceptibility of DHA oligomers for PK digestion as compared to DOPAL-SOs (Figure 2i). The higher stability of DOPAL-SOs could result from the covalent Schiff's base adducts present within the oligomers which may provide tighter binding interactions leading to a more compact structure resistant to enzymatic cleavage. On the contrary,

DHA oligomers, which are formed by both covalent and noncovalent interactions, seem to be less stable. Nevertheless, the data clearly point out that DOPAL-SOs and DHA-SOs are structurally and conformationally different from one another.

Both DOPAL and DHA-Derived  $\alpha$ S Oligomer Differentially Modulate  $A\beta$  Aggregation. We further investigated the ability of DOPAL-SOs and DHA-SOs to cross-seed A $\beta$ 42. To do so, 0.75  $\mu$ M of SEC-fractionated DOPAL-SOs (fraction 17 or 18) were incubated with seed-free, 15  $\mu$ M A $\beta$ 42 monomers and monitored for 48 h by thioflavin-T (ThT) fluorescence. A $\beta$ 42 control in the absence of oligomer seeds showed a sigmoidal ThT fluorescence curve with 10 h of aggregation lag time (Figure 3a). However, the addition of either fraction 17 or 18 of DOPAL-SOs decreased the aggregation by increasing the lag time of  $A\beta$  aggregation to ~35 h along with a decrease in the plateau intensity of ThT fluorescence (Figure 3a). Aliquots of the samples from all three reactions were removed at given time points and analyzed by immunoblotting using Ab5 monoclonal antibody for A $\beta$ 42. Up to 20 h, the samples incubated with DOPAL-SOs showed the presence of predominantly monomers in the immunoblots, while the control A $\beta$  showed the presence of high-molecularweight species (Figure 3b). After 48 h, the control A $\beta$  formed fibrils that failed to enter the gel, but the samples with DOPAL-SOs showed largely monomers with some fibrils mirroring the ThT data (Figure 3b). In parallel, conformational changes of the samples were monitored by far-UV CD. The CD spectra for the  $A\beta$  control also showed a conformational change from a random coil at 7 h of incubation to a  $\beta$ -sheet after 20 h with characteristic minima at 220 nm and maxima at 198 nm (black; Figure 3c-e). Coincubation of fractions 17 and 18 of isolated DOPAL-SOs with A $\beta$  remained in a random coil conformation up to 20 h before converting to

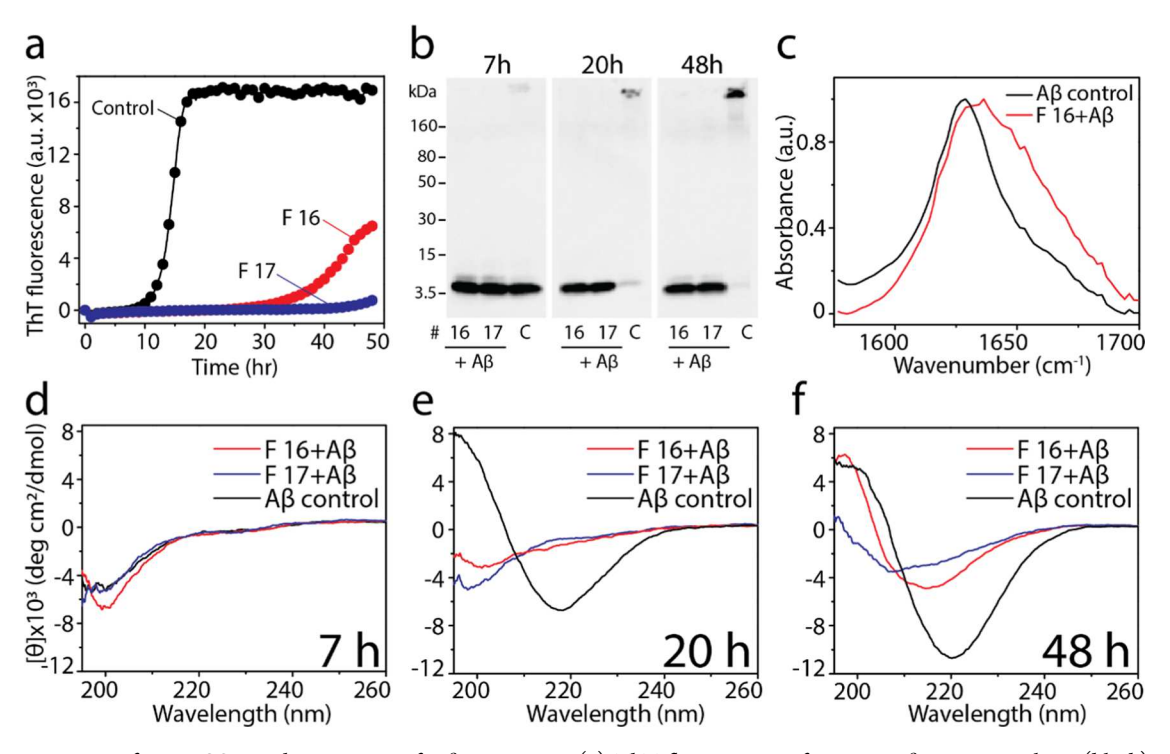


Figure 4. Interaction of DHA-SOs in the presence of  $A\beta$  monomers. (a) ThT fluorescence of 15  $\mu$ M  $A\beta$  monomer alone (black) and in the presence of 0.75  $\mu$ M DHA-SOs corresponding to fraction numbers 16 (red) and 17 (blue). (b) Immunoblotting of ThT reactions (a) at 7, 20, and after 48 h using Ab5 monoclonal antibody; C represents the  $A\beta$  control reaction. (c) FTIR analysis of 15  $\mu$ M  $A\beta$  monomer alone and in the presence of 0.75  $\mu$ M DHA-SOs after 48 h. (d–f) CD spectra of ThT reactions (a) at 7, 20, and 48 h.

a  $\beta$ -sheet after 48 h (red and blue; Figure 3c–e). The fibrils formed at the end of the reaction after 48 h of incubation were sedimented and analyzed with FTIR, which showed the parallel  $\beta$ -sheet-rich structure for both the coincubated reactions and control with a peak centered at 1630 cm<sup>-1</sup> (Figure 3c). These results indicate that DOPAL-SOs delay the aggregation of A $\beta$ 42 but form a similar  $\beta$ -sheet secondary structure of fibrils as the control (Figure 3c). However, these observations do not discount the possibility of having dissimilar structural arrangements as CD and FTIR are inconspicuous to such atomic-level changes.

Next, we investigated interactions between DHA-SOs and A $\beta$ 42 by incubating 0.75  $\mu$ M each of DHA-SO fractions 16 and 17 with freshly prepared, seed-free 15  $\mu$ M A $\beta$ 42 monomers at physiological temperature. ThT fluorescence indicated that the A $\beta$  aggregation was attenuated by the oligomers based on the increase in the lag times observed (Figure 4a). This was also evident from the immunoblots, which showed inhibition of aggregation by both fractions of DHA-SOs as opposed to the control A $\beta$  in the absence of oligomers (Figure 4b). Fibrillar species were not detected in the reactions containing  $A\beta$  monomers coincubated with DHA-SOs. In far-UV CD obtained in parallel, conformational changes of  $A\beta$  in the presence of DHA-SOs with monomer showed a faster conversion from random coiled to  $\beta$ -sheet structure than the control without the oligomers (Figure 4df). However, the DHA-SO coincubated samples showed spectra that were deviated from the ideal  $\beta$ -sheet with a minimum at 220 nm but contained a partial  $\alpha$ - or  $3_{10}$ -helical characteristics with a negative shoulder at 208 nm (red and blue; Figure 4d-f) unlike those with DOPAL-SOs. FTIR analysis of the samples after 48 h confirmed the presence of the  $\beta$ -sheet structure for the A $\beta$  control, while a combination of  $\alpha$ - helical and  $\beta$ -sheet characteristics for the reaction similar to the CD (Figure 4c). Together, these data suggest that DHA-SOs also inhibit  $A\beta$  aggregation but do so by converting  $A\beta$  to a conformation containing a mixture of  $\alpha$ -helical and  $\beta$ -sheet secondary structures.

 $A\beta$  Aggregates Generated from Seeding DOPAL and DHA-Derived aS Oligomers Show Enhanced Neurotoxicity. It is clear from the data presented thus far that both DOPAL-SOs and DHA-SOs have subtle differences that seem to manifest in the way they seed  $A\beta$  aggregation. To see whether these differences manifest in their cellular toxicity, their effects were investigated for cell viability in neuroblastoma cells. First, the reaction containing 15  $\mu$ M A $\beta$  was incubated with and without 0.75 µM DOPAL-SOs or DHA-SOs at 37 °C for 48 h. Aliquots of reaction were diluted twofolds in DMEM/F-12 and control samples containing 7.5  $\mu$ M A $\beta$  monomer, and 325 nM DOPAL-SOs or DHA-SOs were added to SH-SY5Y neuroblastoma cells seeded 24 h prior to the experiment. The toxicity of these species in neuroblastoma cells was examined using XTT cytotoxicity assay (described in the Materials and Methods section). The results indicate the greater toxicity of  $A\beta$  species formed in the presence of the oligomers as compared to their respective controls (Figure 5). A $\beta$  monomers showed the least toxicity among all species, while DHA-SOs in the presence of A $\beta$ showed the highest toxicity (Figure 5). Together, the data suggest the cross-seeding of  $\alpha S$  oligomers with  $A\beta$  augments toxicity.

In this study, we generated two physiologically relevant and conformationally distinct  $\alpha$ S oligomers, DOPAL-SOs or DHA-SOs, which showed subtle biophysical differences and chemically different modes of interaction with A $\beta$ . The results show that the two oligomers interact with and delay the rate of

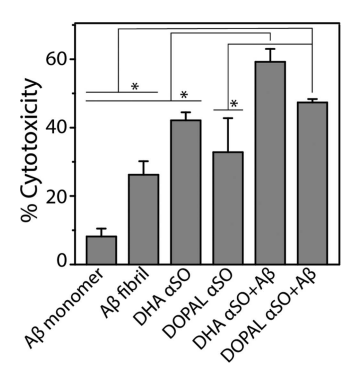


**Figure 5.** Cytotoxicity of DOPAL-SOs and DHA-SOs with and without  $A\beta$  using XTT in mammalian SH-SY5Y neuroblastoma cells. Data were obtained in triplicates; \* represents p < 0.05 using one-way ANOVA analysis.

 $A\beta$  aggregation to different extents. More importantly, the modulation of A $\beta$  aggregation by the two  $\alpha$ S oligomers was accompanied by enhancement in cytotoxicity as compared to either  $A\beta$  alone or DOPAL-SOs or DHA-SOs. Direct interaction of monomeric  $\alpha S$  and  $A\beta$ , oligomeric  $\alpha S$ , and tau in relevance to AD and synucleinopathies has been shown in the previous studies. 20,22 Despite the preponderance of AD in patients with synucleinopathies, the interplay between specific  $\alpha$ S oligomers and A $\beta$ , key constituents of Lewy bodies and plaques, respectively, has remained unexplored. The conformational diversity among amyloid oligomers and their cellular mechanisms have been well established but not in the context of cross-interactions with other amyloid proteins. In this study, we sought to understand the dynamics and cellular effects of cross-interactions between  $\alpha S$  oligomers and  $A\beta$  that has remained elusive. We have previously generated and characterized dopamine-derived  $\alpha S$  oligomers (DSOs) capable of homotypic and heterotypic interactions.<sup>21</sup> In this study, we focused on the more reactive and toxic intermediate of dopamine metabolism, DOPAL. Dopamine is oxidized in the cytoplasm by MAO to toxic DOPAL, which is shown to be upregulated in PD.<sup>32</sup> We also used DHA fatty acid, a major component of myelin that covalently binds to  $\alpha$ S and generate oligomers.30,36

We observed that DOPAL-SOs and DHA-SOs show subtle yet important differences; DHA-SOs have a larger hydrodynamic radius than DOPAL-SOs, both have distinct secondary structures and show differences in stability toward proteinase K digestion. These differences are clearly manifested in the way they interact with  $A\beta$  monomers. While both oligomers delayed A $\beta$  aggregation, DHA-SOs showed more effective inhibition than DOPAL-SOs. Despite the attenuation of aggregation lag times, seeding with DOPAL-SOs still resulted in the formation of high-molecular-weight aggregates at 48 h, unlike DHA-SOs-seeded A $\beta$  species, which remained monomeric as confirmed by the immunoblots. Though DHA-SOs inhibited the formation of ThT-positive high-molecular-weight A $\beta$  aggregates, the presence of lowmolecular-weight oligomers and protofibrils cannot be ruled out. Nonetheless, we observed conformational variability in both species with a mixture of random coiled,  $\alpha$ -helical, and  $\beta$ sheet for DHA-SO-derived A $\beta$  aggregates compared to pure  $\beta$ sheet secondary structure in DOPAL-SO-derived species. These conformational differences could be correlated with their toxicity in SH-SY5Y neuroblastoma cells. While both DHA and DOPAL-SOs were more cytotoxic compared to

controls, their interaction with  $A\beta$  led to a greater degree of toxicity possibly due to the formation of polymorphic  $A\beta$  species. Among all of the samples, DHA-SO-seeded  $A\beta$  displayed the highest degree of toxicity, which is also observed by other research groups previously. This can be attributed to the conformational distinctiveness as well as the presence of different distributions of oligomers and protofibrils at low concentrations between DOPAL-SO- and DHA-SO-seeded reactions.

In sum, the study presented here highlights the molecular basis of interplay and synergism between  $A\beta$  and  $\alpha S$  oligomers that have not been known before. These results help unravel the principle behind cross-interactions among amyloid proteins is that depending on the conformation and properties of oligomers of  $\alpha S$ ,  $A\beta$  monomers seeded by these oligomers may generate a polymorph of  $A\beta$  fibrils with distinctive biophysical and cellular properties as schematically depicted in Figure 6.

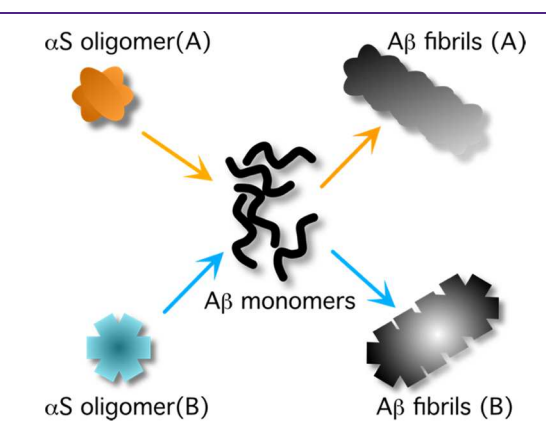


Figure 6. Generalized schematic summary from the results obtained.

These mechanistic insights also help deepen our understanding of the clinical and pathological overlaps observed in AD and synucleinopathies, the one that could arise from the interaction between  $A\beta$  and  $\alpha$ S. Further details of the mechanisms will continue to emerge that could precisely decipher the dynamic interplay between monomers, oligomers, and fibrils of  $A\beta$  and  $\alpha$ S.

# MATERIALS AND METHODS

**Materials.** DOPAL and DHA were purchased from Cayman Chemicals and Sigma-Aldrich, respectively. Monoclonal antibody, Syn211 ( $\alpha$ S specific), was purchased from Millipore Sigma, while AbS was a generous gift from Dr. Levites (University of Florida). All other routine laboratory chemicals and consumables were purchased from Thermo Scientific.

Recombinant Protein Expression and Purification. Recombinant expression and purification of  $\alpha S$  and  $A\beta$  were carried out following previously established protocol. 40,41 Briefly,  $\alpha S$  and  $A\beta 42$  plasmid were transformed and grown in Escherichia coli BL21 (DE3) cells, and protein expression was induced with 1 mM IPTG. For  $\alpha S$ , cells were harvested and lysed in lysis buffer (20 mM Tris, 50 mM NaCl, 10 mM imidazole, pH 8.0) in the presence of PMSF and sonicated using Misonix XL-2000 for eight cycles (45 s brust with 1 min rest). The lysate was centrifuged at 15 000g, and supernatant was loaded into Ni-NTA affinity column. Protein was washed using two sets of wash buffers—wash 1 containing 20 mM Tris, 50 mM NaCl, and 20 mM imidazole and wash 2 containing 20 mM Tris, 50 mM NaCl, and 75 mM imidazole at pH 8.0. The column was further subjected to elution buffer containing 20 mM Tris, 50 mM NaCl, and 250 mM imidazole at pH 8.0. The eluted protein was dialyzed against distilled water for two cycles each of 2 h and lyophilized. The

lyophilized protein was stored at  $-80\,^{\circ}\text{C}$ . Protein was resuspended 50 mM NaOH in Millipore water, incubated for 30 min, and subjected to size exclusion chromatography (SEC) in 20 mM Tris pH 8.0 to obtain monomeric  $\alpha S$ . For  $A\beta$ , harvested cells were lysed in lysis buffer (20 mM Tris Buffer, 1 mM EDTA, pH 8.00) and sonicated for 10 cycles (30 s brust with 1 min rest) followed by centrifugation at 10 000g for 10 min. Pellets were collected and two more rounds of sonication cycle were carried out with eight and six cycles, respectively, followed by centrifugation at 15 000g for 10 min between each step. The pellet was then dissolved in 4 M urea and sonicated for another six cycles. The lysate in urea was centrifuged at 15 000g for 10 min. The supernatant was collected and passed through a 0.2  $\mu$ m to remove any debris. The filtrate was subjected to HPLC, and the obtained A $\beta$  was lyophilized for long-term storage. To freshly purify  $A\beta$  monomers, lyophilized  $A\beta$  was incubated in 10 mM NaOH and subjected to SEC.

Preparation of DOPAL and DHA-Derived αS Oligomers. DOPAL-SOs were prepared by incubating 50  $\mu$ M monomeric αS with 1 mM DOPAL in 20 mM Tris buffer pH 8.0. Similarly, DHA-SOs were prepared by incubating 50  $\mu$ M monomeric αS with 2.5 mM DHA in PBS buffer. Both reactions were incubated at 37 °C in an incubator shaker at 700 rpm for 24 h and subjected to SEC in 20 mM Tris buffer pH 8.0. Isolated oligomer concentration was calculated and characterized using DLS.

**SDS-PAGE and Western Blotting.** Sample aliquots of isolated  $\alpha S$  oligomers and their cross-seeding reaction with  $A\beta$  were subjected to SDS-PAGE and immunoblotting using monoclonal anti- $\alpha S$  antibody, clone syn211 (Millipore Sigma), monoclonal Ab5 antibody as described previously. Briefly, all of the samples were mixed with 4× Laemmli sample loading buffer and loaded onto SDS-PAGE Biorad Mini-PROTEAN 4–20% precast gel. For immunoblotting, gels were transferred onto a 0.45  $\mu$ m Amersham Protran Premium nitrocellulose membrane (GE Life Sciences), and blot was boiled for 1 min in 1× PBS. Blot was incubated overnight in the blocking buffer (5% nonfat dry milk, 1% Tween-20 in 1× PBS) followed by primary antibodies against  $\alpha S$  or  $\alpha S$ , and antimouse secondary antibodies each for 2 h. Blot images were acquired on GelDoc molecular imager (Bio-Rad) after treating with ECL reagent.

**Dynamic Light Scattering.** Dynamic light scattering (DLS) experiments were carried out in a Zetasizer Nano S instrument (Malvern, Inc.). The data were obtained with 70  $\mu$ L of the sample volume by averaging three runs each of 10 s with pre-equilibration time of 30 s. All of the parameters were determined, autocorrelation function was plotted as a function of time, diameter was calculated using volume (%) function, and plotted in origin 8.5.

**Circular Dichroism.** Circular dichroism (CD) spectra of respective samples were measured in 20  $\mu$ M Tris buffer pH 8.0 in the far-UV region in a Jasco J-815 spectrophotometer (Jasco MD) using the established protocol.<sup>43</sup>

Fourier Transform Infrared (FTIR) Spectroscopy. The samples of monomeric proteins, DOPAL and DHA-derived  $\alpha S$  oligomers, and fibrils from the cross-seeding reaction were lyophilized and dissolved in  $D_2O$  and measured in a Cary 630 FTIR spectrometer. FTIR spectra were acquired with 1024 total scans from 1800 to 1400 cm<sup>-1</sup> at a resolution of 4 cm<sup>-1</sup>. Spectra were blank subtracted with  $D_2O$ , normalized, and plotted in Origin 8.5.

**Thioflavin-T (ThT) Binding Assay.** ThT aggregation kinetics was performed by incubating the samples with 10  $\mu$ M ThT, and data were monitored using a BioTek Synergy H1 microplate reader at 37 °C. Samples excitation and emission were set as 452 and 485 nm, respectively. Data were plotted as ThT fluoresncence versus time in Origin 8.5.

**Proteinase K Digestion.** DOPAL-SOs and DHA-SOs (13.3  $\mu$ g) were digested with 0.9 ng of proteinase K (PK) diluted from a stock of 20 mg/mL (Ambion, Inc.). Reactions were run at 37 °C by shaking at 200 rpm, and aliquots of the reaction were quenched with 0.5 mM PMSF at 10, 20, 30, and 40 min, respectively. Post quenching, 9.95 ng of reaction samples were run in a Invitrogen 4–12% SDS-PAGE gel and transferred onto an 0.2  $\mu$ m nitrocellulose membrane. Protein bands were investigated using anti- $\alpha$ S monoclonal antibody (Syn211,

Millipore Sigma) and antimouse horse radish peroxidase secondary antibody. The immunoblots were imaged with Super Signal West Pico Chemiluminescent Substrate kit (Thermo Fisher Scientific).

**Cell Viability.** Cell viability assay was carried out using 2,3-bis(2-methoxy-4-nitro-5-sulfophenyl)-5-[(phenylamino)carbonyl]-2H-tetrazolium hydroxide (XTT) in SH-SYSY cells as described in our previously established protocols. 40,43 Briefly, human neuroblastoma SH-SYSY was maintained at 37 °C with 5.5% CO<sub>2</sub> in DMEM/F-12 (1:1) media containing 10% FBS and 1% penicillin/streptomycin. Cells were plated in 96-well plates 24 h prior to the experiment and treated with respective samples. After incubating the samples for 24 h prior, both the blank and experimental readings were obatined in a BioTek Synergy H1 microplate reader.

### AUTHOR INFORMATION

### **Corresponding Author**

Vijayaraghavan Rangachari — Department of Chemistry and Biochemistry, School of Mathematics and Natural Sciences and Center for Molecular and Cellular Biosciences, University of Southern Mississippi, Hattiesburg, Mississippi 39406, United States; orcid.org/0000-0003-4087-5947; Email: vijay.rangachari@usm.edu

### **Authors**

Shailendra Dhakal — Department of Chemistry and Biochemistry, School of Mathematics and Natural Sciences, University of Southern Mississippi, Hattiesburg, Mississippi 39406, United States

Jhinuk Saha — Department of Chemistry and Biochemistry, School of Mathematics and Natural Sciences, University of Southern Mississippi, Hattiesburg, Mississippi 39406, United States

Courtney E. Wyant – Department of Chemistry and Biochemistry, School of Mathematics and Natural Sciences, University of Southern Mississippi, Hattiesburg, Mississippi 39406, United States

Complete contact information is available at: https://pubs.acs.org/10.1021/acschemneuro.1c00530

# **Author Contributions**

V.R. conceptualized the project; S.D. performed protein purification, biophysical experiments along with C.E.W.; S.D. also conducted the cell culture experiments; and J.S. conducted proteinase K digestion and collected FTIR data. V.R., S.D., and J.S. participated in intellectual discussions and manuscript writing and editing.

# Notes

The authors declare no competing financial interest.

### ACKNOWLEDGMENTS

The authors would like to thank the following agencies for financial support: National Institute of Aging (1R56AG062292-01), National Institute of General Medical Sciences (R01GM120634), and the National Science Foundation (NSF CBET 1802793) to V.R. The authors also thank the National Center for Research Resources (5P20RR01647-11) and the National Institute of General Medical Sciences (8 P20 GM103476-11) from the National Institutes of Health for funding through INBRE for the use of their core facilities.

# REFERENCES

(1) Armstrong, R. A.; Lantos, P. L.; Cairns, N. J. Overlap between neurodegenerative disorders. *Neuropathology* **2005**, *25*, 111–124.

- (2) Armstrong, R. A.; et al. On the 'classification' of neuro-degenerative disorders: discrete entities, overlap or continuum? *Folia Neuropathol.* **2012**, *50*, 201–218.
- (3) Jellinger, K. A. Interaction between pathogenic proteins in neurodegenerative disorders. J. Cell. Mol. Med. 2012, 16, 1166–1183.
- (4) Irwin, D. J.; Lee, V. M.-Y.; Trojanowski, J. Q. Parkinson's disease dementia: convergence of  $\alpha$ -synuclein, tau and amyloid- $\beta$  pathologies. *Nat. Rev. Neurosci.* **2013**, *14*, 626–636.
- (5) Lippa, C. F.; Schmidt, M. L.; Lee, V. M.-Y.; Trojanowski, J. Q.  $\alpha$ -Synuclein in familial Alzheimer disease: epitope mapping parallels dementia with Lewy bodies and Parkinson disease. *Arch. Neurol.* **2001**, *58*, 1817–1820.
- (6) Rosen, A. R.; Steenland, N. K.; Hanfelt, J.; Factor, S. A.; Lah, J. J.; Levey, A. I. Evidence of shared risk for Alzheimer's disease and Parkinson's disease using family history. *Neurogenetics* **2007**, *8*, 263–270.
- (7) Martl, M. J.; Tolosa, E.; Campdelacreu, J. Clinical overview of the synucleinopathies. *Mov. Disord.* **2003**, *18*, 21–27.
- (8) Bloom, G. S. Amyloid- $\beta$  and tau: the trigger and bullet in Alzheimer disease pathogenesis. *JAMA Neurol.* **2014**, 71, 505–508.
- (9) Giacobini, E.; Gold, G. Alzheimer disease therapy—moving from amyloid- $\beta$  to tau. *Nat. Rev. Neurosci.* **2013**, *9*, 677–686.
- (10) Baier, M.; Apelt, J.; Riemer, C.; Gültner, S.; Schwarz, A.; Bamme, T.; Burwinkel, M.; Schliebs, R. Prion infection of mice transgenic for human APPSwe: increased accumulation of cortical formic acid extractable  $A\beta$  (1–42) and rapid scrapie disease development. *Int. J. Dev. Neurosci.* **2008**, 26, 821–824.
- (11) Tan, R. H.; Kril, J. J.; Yang, Y.; Tom, N.; Hodges, J. R.; Villemagne, V. L.; Rowe, C. C.; Leyton, C. E.; Kwok, J. B.; Ittner, L. M.; et al. Assessment of amyloid  $\beta$  in pathologically confirmed frontotemporal dementia syndromes. *Alzheimer's Dement.* **2017**, 9, 10-20.
- (12) Calingasan, N. Y.; Chen, J.; Kiaei, M.; Beal, M. F.  $\beta$ -amyloid 42 accumulation in the lumbar spinal cord motor neurons of amyotrophic lateral sclerosis patients. *Neurobiol. Dis.* **2005**, *19*, 340–347.
- (13) Yoon, E. J.; Park, H.-J.; Kim, G.-Y.; Cho, H.; Choi, J.-H.; Park, H.-Y.; Jang, J.-Y.; Rhim, H.; Kang, S. Intracellular amyloid beta interacts with SOD1 and impairs the enzymatic activity of SOD1: implications for the pathogenesis of amyotrophic lateral sclerosis. *Exp. Mol. Med.* **2009**, *41*, 611–617.
- (14) Hepp, D. H.; Vergoossen, D. L.; Huisman, E.; Lemstra, A. W.; Berendse, H. W.; Rozemuller, A. J.; Foncke, E. M.; van de Berg, W. D. Distribution and load of amyloid- $\beta$  pathology in Parkinson disease and dementia with Lewy bodies. *J. Neuropathol. Exp. Neurol.* **2016**, 75, 936–945.
- (15) Parkkinen, L.; Soininen, H.; Alafuzoff, I. Regional distribution of  $\alpha$ -synuclein pathology in unimpaired aging and Alzheimer disease. *J. Neuropathol. Exp. Neurol.* **2003**, *62*, 363–367.
- (16) Hamilton, R. L. Lewy bodies in Alzheimer's disease: a neuropathological review of 145 cases using  $\alpha$ -synuclein immunohistochemistry. *Brain Pathol.* **2000**, *10*, 378–384.
- (17) Yamada, T.; Itoh, K.; Matsuo, K.; Yamamoto, Y.; Hosokawa, Y.; Koizumi, T.; Shiga, K.; Mizuno, T.; Nakagawa, M.; Fushiki, S. Concomitant alpha-synuclein pathology in an autopsy case of amyotrophic lateral sclerosis presenting with orthostatic hypotension and cardiac arrests. *Neuropathology* **2014**, *34*, 164–169.
- (18) Doherty, M.; Bird, T.; Leverenz, J. α-Synuclein in motor neuron disease: an immunohistologic study. *Acta Neuropathol.* **2004**, 107, 169–175.
- (19) Irwin, D. J.; Hurtig, H. I. The contribution of tau, amyloid-beta and alpha-synuclein pathology to dementia in Lewy body disorders. *J. Alzheimer's Dis. Parkinsonism* **2018**, 8, No. 444.
- (20) Köppen, J.; Schulze, A.; Machner, L.; Wermann, M.; Eichentopf, R.; Guthardt, M.; Hähnel, A.; Klehm, J.; Kriegeskorte, M.-C.; Hartlage-Rübsamen, M.; et al. Amyloid-beta peptides trigger aggregation of alpha-synuclein in vitro. *Molecules* **2020**, *25*, No. S80.

- (21) Planchard, M. S.; Exley, S. E.; Morgan, S. E.; Rangachari, V. Dopamine-induced  $\alpha$ -synuclein oligomers show self-and cross-propagation properties. *Protein Sci.* **2014**, 23, 1369–1379.
- (22) Sengupta, U.; Puangmalai, N.; Bhatt, N.; Garcia, S.; Zhao, Y.; Kayed, R. Polymorphic  $\alpha$ -synuclein strains modified by dopamine and docosahexaenoic acid interact differentially with tau protein. *Mol. Neurobiol.* **2020**, *57*, 2741–2765.
- (23) Nekooki-Machida, Y.; Kurosawa, M.; Nukina, N.; Ito, K.; Oda, T.; Tanaka, M. Distinct conformations of in vitro and in vivo amyloids of huntingtin-exon1 show different cytotoxicity. *Proc. Natl. Acad. Sci. U.S.A.* **2009**, *106*, 9679–9684.
- (24) Ladiwala, A. R. A.; Litt, J.; Kane, R. S.; Aucoin, D. S.; Smith, S. O.; Ranjan, S.; Davis, J.; Van Nostrand, W. E.; Tessier, P. M. Conformational differences between two amyloid  $\beta$  oligomers of similar size and dissimilar toxicity. *J. Biol. Chem.* **2012**, 287, 24765–24773.
- (25) Toyama, B. H.; Weissman, J. S. Amyloid structure: conformational diversity and consequences. *Annu. Rev. Biochem.* **2011**, *80*, 557–585.
- (26) Follmer, C. Monoamine oxidase and  $\alpha$ -synuclein as targets in Parkinson's disease therapy. *Expert Rev. Neurother.* **2014**, *14*, 703–716
- (27) Panneton, W. M.; Kumar, V.; Gan, Q.; Burke, W. J.; Galvin, J. E. The neurotoxicity of DOPAL: behavioral and stereological evidence for its role in Parkinson disease pathogenesis. *PLoS One* **2010**, *5*, No. e15251.
- (28) Follmer, C.; Coelho-Cerqueira, E.; Yatabe-Franco, D. Y.; Araujo, G. D.; Pinheiro, A. S.; Domont, G. B.; Eliezer, D. Oligomerization and membrane-binding properties of covalent adducts formed by the interaction of  $\alpha$ -synuclein with the toxic dopamine metabolite 3, 4-dihydroxyphenylacetaldehyde (DOPAL). *J. Biol. Chem.* **2015**, 290, 27660–27679.
- (29) Burke, W. J.; Li, S. W.; Williams, E. A.; Nonneman, R.; Zahm, D. S. 3, 4-Dihydroxyphenylacetaldehyde is the toxic dopamine metabolite in vivo: implications for Parkinson's disease pathogenesis. *Brain Res.* **2003**, *989*, 205–213.
- (30) De Franceschi, G.; Frare, E.; Pivato, M.; Relini, A.; Penco, A.; Greggio, E.; Bubacco, L.; Fontana, A.; de Laureto, P. P. Structural and morphological characterization of aggregated species of  $\alpha$ -synuclein induced by docosahexaenoic acid. *J. Biol. Chem.* **2011**, 286, 22262–22274.
- (31) Fecchio, C.; De Franceschi, G.; Relini, A.; Greggio, E.; Dalla Serra, M.; Bubacco, L.; de Laureto, P. P.  $\alpha$ -Synuclein oligomers induced by docosahexaenoic acid affect membrane integrity. *PLoS One* **2013**, *8*, No. e82732.
- (32) Masato, A.; Plotegher, N.; Boassa, D.; Bubacco, L. Impaired dopamine metabolism in Parkinson's disease pathogenesis. *Mol. Neurodegener.* **2019**, *14*, No. 35.
- (33) De Franceschi, G.; Frare, E.; Bubacco, L.; Mammi, S.; Fontana, A.; de Laureto, P. P. Molecular insights into the interaction between  $\alpha$ -synuclein and docosahexaenoic acid. *J. Mol. Biol.* **2009**, 394, 94–107.
- (34) van Diggelen, F.; Hrle, D.; Apetri, M.; Christiansen, G.; Rammes, G.; Tepper, A.; Otzen, D. E. Two conformationally distinct  $\alpha$ -synuclein oligomers share common epitopes and the ability to impair long-term potentiation. *PLoS One* **2019**, *14*, No. e0213663.
- (35) Broersen, K.; Van Den Brink, D.; Fraser, G.; Goedert, M.; Davletov, B.  $\alpha$ -Synuclein adopts an  $\alpha$ -helical conformation in the presence of polyunsaturated fatty acids to hinder micelle formation. *Biochemistry* **2006**, *45*, 15610–15616.
- (36) Kao, Y.-C.; Ho, P.-C.; Tu, Y.-K.; Jou, I.; Tsai, K.-J. Lipids and Alzheimer's disease. *Int. J. Mol. Sci.* **2020**, *21*, No. 1505.
- (37) Verma, M.; Vats, A.; Taneja, V. Toxic species in amyloid disorders: Oligomers or mature fibrils. *Ann. Indian Acad. Neurol.* **2015**, *18*, 138.
- (38) Granzotto, A.; Bolognin, S.; Scancar, J.; Milacic, R.; Zatta, P. Beta-amyloid toxicity increases with hydrophobicity in the presence of metal ions. *Monatsh. Chem.* **2011**, *142*, 421–430.

- (39) Mannini, B.; Mulvihill, E.; Sgromo, C.; Cascella, R.; Khodarahmi, R.; Ramazzotti, M.; Dobson, C. M.; Cecchi, C.; Chiti, F. Toxicity of protein oligomers is rationalized by a function combining size and surface hydrophobicity. *ACS Chem. Biol.* **2014**, 9, 2309–2317.
- (40) Dhakal, S.; Wyant, C. E.; George, H. E.; Morgan, S. E.; Rangachari, V. Prion-like C-terminal domain of TDP-43 and  $\alpha$ -Synuclein interact synergistically to generate neurotoxic hybrid fibrils. *J. Mol. Biol.* **2021**, 433, No. 166953.
- (41) Yoo, S.; Zhang, S.; Kreutzer, A. G.; Nowick, J. S. An efficient method for the expression and purification of  $A\beta$  (M1–42). *Biochemistry* **2018**, *57*, 3861–3866.
- (42) Dhakal, S.; Sapkota, K.; Huang, F.; Rangachari, V. Cloning, expression and purification of the low-complexity region of RanBP9 protein. *Protein Expression Purif.* **2020**, *172*, No. 105630.
- (43) Saha, J.; Dean, D. N.; Dhakal, S.; Stockmal, K. A.; Morgan, S. E.; Dillon, K. D.; Adamo, M. F.; Levites, Y.; Rangachari, V. Biophysical characteristics of lipid-induced  $A\beta$  oligomers correlate to distinctive phenotypes in transgenic mice. *FASEB J.* **2021**, *35*, No. e21318.